Clinical Cancer Research

Repurposing Tin Mesoporphyrin as an Immune Checkpoint Inhibitor Shows Therapeutic Efficacy in Preclinical Models of Cancer

Tamara Muliaditan[1], James W. Opzoomer[1], Jonathan Caron[1], Mary Okesola[1], Paris Kosti[1], Sharanpreet Lall[1], Mieke Van Hemelrijck[2], Francesco Dazzi[1], Andrew Tutt[3], Anita Grigoriadis[3], Cheryl E. Gillett[1], Stephen F. Madden[4], Joy M. Burchell[1], Shahram Kordasti[5], Sandra S. Diebold[1], James F. Spicer[1], and James N. Arnold[1]

Abstract

Purpose: Unprecedented clinical outcomes have been achieved in a variety of cancers by targeting immune checkpoint molecules. This preclinical study investigates heme oxygenase-1 (HO-1), an immunosuppressive enzyme that is expressed in a wide variety of cancers, as a potential immune checkpoint target in the context of a chemotherapy-elicited antitumor immune response. We evaluate repurposing tin mesoporphyrin (SnMP), which has demonstrated safety and efficacy targeting hepatic HO in the clinic for the treatment of hyperbilirubinemia, as an immune checkpoint blockade therapy for the treatment of cancer.

Experimental Design: SnMP and genetic inactivation of myeloid HO-1 were evaluated alongside 5-fluorouracil in an aggressive spontaneous murine model of breast cancer (*MMTV-PyMT*). Single-cell RNA sequencing analysis, tumor microarray, and clinical survival data from breast cancer patients were used to support the clinical relevance of our observations.

Results: We demonstrate that SnMP inhibits immune suppression of chemotherapy-elicited $CD8^+$ T cells by targeting myeloid HO-1 activity in the tumor microenvironment. Microarray and survival data from breast cancer patients reveal that HO-1 is a poor prognostic factor in patients receiving chemotherapy. Single-cell RNA-sequencing analysis suggests that the myeloid lineage is a significant source of HO-1 expression, and is co-expressed with the immune checkpoints PD-L1/2 in human breast tumors. *In vivo*, we therapeutically compare the efficacy of targeting these two pathways alongside immune-stimulating chemotherapy, and demonstrate that the efficacy of SnMP compares favorably with PD-1 blockade in preclinical models.

Conclusions: SnMP could represent a novel immune checkpoint therapy, which may improve the immunological response to chemotherapy. *Clin Cancer Res; 24(7); 1617–28. ©2018 AACR.*

Introduction

Unparalleled clinical responses have been achieved in cancer patients using antibodies which block the immune checkpoint molecules PD-1 and CTLA-4 to prevent $CD8^+$ T-cell anergy in the tumor microenvironment (1). Combining PD-1 and CTLA-4 blockade therapies improves the overall clinical response compared with the monotherapies (2), highlighting the complementary effects of these checkpoint molecules. However, the absence of a clinical response in a significant proportion of patients suggests that further therapeutic interventions might be required to account for the number and hierarchy of immune checkpoint pathways (2, 3), as well as for the adaptive immune checkpoint response of the tumor (4).

The heme oxygenase (HO) family of proteins is responsible for the breakdown of heme, which is released from dying cells, to the biologically active products biliverdin, ferrous iron (Fe^{2+}) and carbon monoxide (CO; ref. 5). There are two members of the family expressed in humans and mice: HO-1 which is induced in response to stress stimuli, and HO-2 which is constitutively expressed at basal levels in all cells (5, 6). HO-1 has been implicated in many studies to have pro-tumoral properties, including cytoprotection and immune suppression (5, 7–12). Many of these effects have been attributed to CO due to its ability to modulate several signaling pathways including p38 MAPK (13), STAT1/3 (14), and NFκB (15, 16). NFκB in particular is vital for $CD8^+$ T-cell effector function (17). As such, HO activity can compromise antitumor $CD8^+$ T-cell responses in the tumor microenvironment (7).

HO activity has yet to be targeted in the clinic for the treatment of cancer. SnMP is a potent HO inhibitor that targets both HO-1

[1]School of Cancer and Pharmaceutical Sciences, King's College London, Faculty of Life Sciences and Medicine, Guy's Hospital, London, United Kingdom. [2]Translational Oncology and Urology Research, School of Cancer and Pharmaceutical Sciences, King's College London, Faculty of Life Sciences and Medicine, Guy's Hospital, London, United Kingdom. [3]Breast Cancer Now Unit, School of Cancer and Pharmaceutical Sciences, King's College London, Faculty of Life Sciences and Medicine, Guy's Hospital, London, United Kingdom. [4]Population Health Sciences Division, Royal College of Surgeons in Ireland, Ireland. [5]Department of Hematological Medicine, King's College London, School of Cancer and Pharmaceutical Sciences, Faculty of Life Sciences and Medicine, Denmark Hill, London, United Kingdom.

Note: Supplementary data for this article are available at Clinical Cancer Research Online (http://clincancerres.aacrjournals.org/).

J.W. Opzoomer and J. Caron contributed equally to this article.

Current address for S.S. Diebold: National Institute for Biological Standards and Control, Potters Bar, Hertfordshire, EN6 3QG, United Kingdom.

Corresponding Author: James Arnold, King's College London, Guy's Campus, London SE1 1UL. Phone: 44 (0) 20 7848 6415; E-mail: james.n.arnold@kcl.ac.uk

doi: 10.1158/1078-0432.CCR-17-2587

Translational Relevance

Despite nearly 40 years of research describing the tumor-promoting properties of HO-1, it has yet to be evaluated clinically as a therapeutic target. In this study, we evaluate HO-1 as an immune checkpoint. We demonstrate that repurposing the HO-1 inhibitor tin mesoporphyrin (SnMP) as a novel checkpoint therapy in combination with chemotherapy can permit robust immunological control of tumor growth in preclinical models. SnMP has previously demonstrated tolerability and efficacy in the clinic for the treatment of hyperbilirubinemia. We show that HO-1 expression is a poor prognostic factor in breast cancer patients receiving chemotherapy. HO-1 can be co-expressed within the tumor microenvironment with the immune checkpoint molecules PD-L1/2, both in human breast cancer and preclinical models. *In vivo*, we show that the therapeutic efficacy of SnMP compares favorably with anti-PD-1 blockade within chemotherapy regimens. Our data support the clinical evaluation of SnMP as an immune checkpoint therapeutic in cancer therapy.

and HO-2 (18), and has been administered to infants to target hepatic HO activity to control excessive serum bilirubin levels for conditions such as neonatal jaundice and Crigler-Najjar syndrome (19, 20). However, despite this, very few published studies have used SnMP to target HO-1 in the cancer field. SnMP does not affect tumor growth in ectopic Lewis lung carcinomas as a single agent in murine models, unless ovalbumin is artificially introduced into the tumor to raise a robust antitumor immune response (7).

As such, repurposing SnMP for the treatment of cancer is an attractive route to target the pro-tumoral properties of this enzyme. However, for clinical efficacy it is expected that SnMP would need to be combined with an immune-stimulating agent or therapy. Chemotherapeutics can both prime antitumor $CD8^+$ T-cells and elicit their infiltration into the tumor microenvironment (21–24). Because of their widespread administration in cancer, these compounds may provide the appropriate immunological setting to target the immune-suppressive activity of HO-1.

In this preclinical study we demonstrate, using a chemotherapy-elicited antitumor immune response in a spontaneous murine model of mammary adenocarcinoma (*MMTV-PyMT*), that SnMP can be used as an immune checkpoint therapy that targets myeloid-derived HO-1 to permit immunological control of tumor growth when combined with chemotherapy. We show that *HMOX1* expression is a poor prognostic factor in patients receiving chemotherapy and present data to suggest that HO-1 can be hierarchically equal or more important than the clinically targeted immune checkpoint PD-1 in certain tumor microenvironments, underlining the need to evaluate SnMP as an immune checkpoint therapy in the treatment of cancer.

Materials and Methods

Mice

MMTV-PyMT mice used in this study were on a FVB/n background. The *Hmox1*$^{fl/fl}$ (25) and *Itgam*^{cre}(26) transgenic mice were on a C57Bl/6 background and a gift from Professor George Kollias, Biomedical Sciences Research Center "Alexander Fleming," Athens, Greece. These mice were crossed to generate the *MMTV-PyMT*, *Hmox1*$^{fl/fl}$, *Itgam*$^{cre+/-}$ line, which was of mixed background. Cohort sizes were informed by prior studies (7). All mice used for experiments were female and randomly assigned to treatment groups. Mice were approximately 26 g when tumors arose. Experiments were performed in at least duplicate and for spontaneous tumor studies individual mice were collected on separate days and all data points are presented. All experiments involving animals were executed in compliance with Institutional and Home Office UK guidelines and regulations (licence 70/7654).

Tumor studies

In studies using *MMTV-PyMT* mice the primary tumor growth was presented. Sn (IV) mesoporphyrin IX dichloride (SnMP; Frontier Scientific) was dissolved and administered as previously described (7). 5-fluorouracil (Sigma-Aldrich) was dissolved in saline. Anti-mouse PD-1 (RMP1-14; Biolegend) was administered at 12 mg/kg every 3 days. Immune-depleted mice were injected every 5 days, starting 48 hours before the commencement of treatment, with 400 μg of either anti-CD8α (53-6.7) or isotype control rat IgG2a (2A3Clone; eBioscience). All drugs were freshly prepared on the day of injection, and administered by intraperitoneal injection. Tumor tissue was enzyme-digested to release single cells as previously described (27).

Tissue staining

Sections of fresh-frozen human breast adenocarcinoma or mouse mammary tumors embedded in OCT were fixed in 4% paraformaldehyde in PBS for 10 minutes at RT. For histology, sections were washed in Tris Buffered Saline; Tween 20, 0.05% (TBST) and blocked with 10% donkey serum (Sigma-Aldrich), 0.2% Triton X-100. HO-1 was detected using 1:100 anti-HO-1 (412811; R&D Systems) and 1:200 anti-rat IgG HRP (Thermo Fisher Scientific) and developed using 3,3′-diaminobenzidine (Thermo Fisher Scientific). Slides were counterstained with hematoxylin, dehydrated, and scanned using a NanoZoomer Digital Slide Scanner (Hamamatsu). Immunofluorescence was performed as previously described (10). The following antibodies and dilutions were used: F4/80, 1:100 (C1:A3-1, Bio-RAD), HO-1, 1:100 (EP1391Y, Origene), CD3, 1:100 (SP7, Abcam), CD8, 1:100 (1:1 ratio of YTS169.4 and 53-6.7; Thermo Fisher Scientific), CD11b, 1:100 (ICRF44, eBioscience), CD14, 1:100 (61D3, eBioscience). Primary antibodies were detected using antigen-specific Donkey IgG, used at 1:200: AlexaFluor 488 anti-rabbit IgG, AlexaFluor 488 anti-rat IgG, AlexaFluor 647 anti-mouse IgG, AlexaFluor 647 anti-rabbit IgG, all of which were purchased from Thermo Fisher Scientific. Nuclei were stained using 1.25 μg/mL 4′,6-diamidino-2-phenylindole, dihydrochloride (DAPI; Thermo Fisher Scientific). Images were acquired using a Nikon Eclipse Ti-E Inverted spinning disk confocal with associated NIS Elements software.

Flow cytometry

Flow cytometry was performed as previously described (7). The following antibodies were purchased from eBioscience and were used at 1 μg/mL unless stated otherwise: Anti- B220 APC (RA3-6B2), CD3ε APC and PE (145-2C11), CD4 FITC (RM4-5), CD8α eFluor 450 (53-6.7), CD8β FITC and eFluor 450 (H35-17.2), CD11b eFluor 450 (M1/70), and CD11b Brilliant Violet 510 (M1/70; Biolegend), CD11c APC (N418), CD16/32 (2.4G2;

Tonbo Biosciences), CD19 APC (6D5; Biolegend), CD45 APC-eFluor 780 (30-F11), CD90.2 eFluor 450 (53-2.1), CD273 PE (B7-DC), CD274 PE (B7-H1), CD279 APC (J43), F4/80 PE (BM8), Granzyme B PE (NGZB) IFN-γ APC (XMG1.2), Ly6C PE (HK1.4), Ly6G APC and FITC (1A8; Biolegend), NK1.1 APC (PK136), TNF PE (MP6-XT22). Where stated, the following corresponding isotype control antibodies at equivalent concentrations to that of the test stain were used: goat IgG APC and PE (Bio-techne), rat IgG2b APC and eFluor 450 (eB149/10H5), rat IgG2a APC and PE (eBR2a) and Armenian Hamster IgG APC (eBio299Arm). Intracellular stains were performed as previously described (7). Dead cells and red blood cells were excluded using 1 μg/mL 7-amino actinomycin D (Sigma-Aldrich) or Fixable Viability Dye eFluor 780 (eBioscience) alongside anti-Ter-119 PerCP-Cy5.5 (Ter-119; eBioscience). Data were collected on a BD FACSCanto II (BD Biosciences). Data were analyzed using FlowJo software (Freestar Inc.). Immune cells ($CD45^+$) were separated based upon the following surface characteristics: $CD11c^+$ $F4/80^-$ (dendritic cells), $CD11b^+$ $F4/80^{hi}$ (macrophages), $CD11b^+$ $F4/80^{low}$ $Ly6G^-$ $Ly6C^+$ (monocytes), $CD11b^+$ $Ly6G^+$ (neutrophils), $NK1.1^+$ $CD3\varepsilon^-$ (NK cells), $NK1.1^+$, $CD3\varepsilon^+$ (NKT cells), $CD3\varepsilon^+$ (T cells), $CD3\varepsilon^+$ $CD4^+$ ($CD4^+$ T cells), $CD3\varepsilon^+$ $CD8\alpha/\beta^+$ ($CD8^+$ T cells), $CD19^+$ (B cells). Cancer-associated fibroblasts (CAF) were identified as $CD45^-$ $Thy1^+$ cells.

Quantitative reverse transcriptase PCR

mRNA was extracted and quantitative reverse transcription PCR was performed as previously described (7) using the EXPRESS one-step Superscript RT PCR kit and the following primers/probes purchased from Thermo Fisher Scientific: *Cxcl9* mm00434946_m1, *Cxcl10* mm00445235_m1, *Cxcl11* mm00444662_m1, *Tbp* mm01277045_m1. Expression of all genes is represented relative to the house-keeping gene Tata-binding protein (*Tbp*). Assays were performed using an ABI 7900HT Fast Real Time PCR instrument (Thermo Fisher Scientific).

Breast cancer patient transcriptomic data

Patient survival data were acquired from the BreastMark dataset (28), the Kaplan–Meier plotter (29–31), and the NCBI Gene Expression Omnibus, accession number GSE65904 (32). Expression data were acquired from the Molecular Taxonomy of Breast Cancer International Consortium (METABRIC; ref. 33). Heat maps were created with Gene Cluster 3.0 and Treeview Software. The single-cell RNA-seq (34) dataset was extracted from the NCBI GEO, accession code GSE75688. Data were acquired as raw gene expression in transcripts per million (TPM). Low-quality cells were filtered from the dataset based upon a threshold of 2000 unique genes detected per cell. Genes that were detected in <2% of single cells were removed leaving 509 cells and 19,097 genes. Data were log transformed [log(TPM + 1)] for all further analyses, which were performed using the R software package Seurat (https://github.com/satijalab/seurat; http://satijalab.org/seurat/). See Supplementary Methods for a detailed description of the single-cell RNASeq analysis pipeline.

Statistical analysis

Normality and homogeneity of variance were determined using a Shapiro–Wilk normality test and a F-test, respectively. Statistical significance was then determined using a two-sided unpaired Students *t* test for parametric, or Mann–Whitney test for nonparametric data using GraphPad Prism 6 software. When comparing paired data, a paired ratio Student *t* test was performed. A Welch's correction was applied when comparing groups with unequal variances. Statistical analysis of tumor growth curves was performed using the "compareGrowthCurves" function of the statmod software package (35). No outliers were excluded from any data presented.

Study approval

The use of animals for this study was approved by the Ethical Review Committee at King's College London and the Home Office, UK. Human breast adenocarcinoma tissue was obtained with informed consent under ethical approval from the King's Health Partners Cancer Biobank (REC reference 12/EE/0493).

Results

SnMP synergizes with 5-FU to control tumor growth in an aggressive spontaneous model of breast cancer

To evaluate the potential clinical efficacy of SnMP on tumor growth, we used the aggressive spontaneous murine model of mammary adenocarcinoma (*MMTV-PyMT*; ref. 36). This preclinical model closely follows the stages to malignancy that occur in human cancer progression (37). HO-1^+ cells could be detected by IHC in *MMTV-PyMT* tumors (Fig. 1A and Supplementary Fig. S1A). These cells accounted for 2.0% ± 1.1% of the tumor (Fig. 1B). HO-1^+ cells were primarily detected as clusters across the stroma, but there was no obvious anatomical location within the tumor in which these cells were predominanly found (Fig. 1A and Supplementary Fig. S1A). All tumors analyzed expressed *Hmox1*, the gene for HO-1, although to varying degrees (Supplementary Fig. S1B), which was in agreement with the IHC analysis. *MMTV-PyMT* mice bearing established spontaneous mammary adenocarcinomas were treated with the HO inhibitor SnMP or with vehicle, and their tumor growth was monitored therafter (Fig. 1C). SnMP did not affect tumor growth in this model, consistent with that observed in ectopic murine Lewis Lung carcinomas (7). Treatment with 5-FU, a chemotherapeutic which has been used in the clinic (38), and which has been demonstrated to stimulate an antitumor immune response (39, 40), also did not affect tumor growth as a single agent (Fig. 1C). Chemotherapy has been described to upregulate HO-1 expression (8, 12), but this was not observed with 5-FU (Supplementary Fig.S1B). When SnMP and 5-FU were concurrently administered there was striking therapeutic synergy between these two drugs, resulting in immediate tumor regression and control of tumor growth (Fig. 1C). These data demonstrate that SnMP could be used to improve responses to chemotherapy.

HO is an immune checkpoint in breast cancer

HO-1 has been demonstrated to modulate the tumor cell stress response (8–12) and to suppress immune-mediated cytotoxicity (11) in response to chemotherapy treatment. To establish whether the tumor control was immunological, SnMP and 5-FU were administered to mice that had been depleted of $CD8^+$ T-cells *in vivo* before the initiation of treatment. This depletion resulted in a loss of tumor-infiltrating $CD8^+$ T-cells (Supplementary Fig. S2A and S2B). Administration of anti-CD8α antibodies resulted in a slowing of tumor growth that became evident at the later stages (Fig. 2A). However, the regression and long-term control of tumor growth seen with SnMP and 5-FU treatment was lost in the

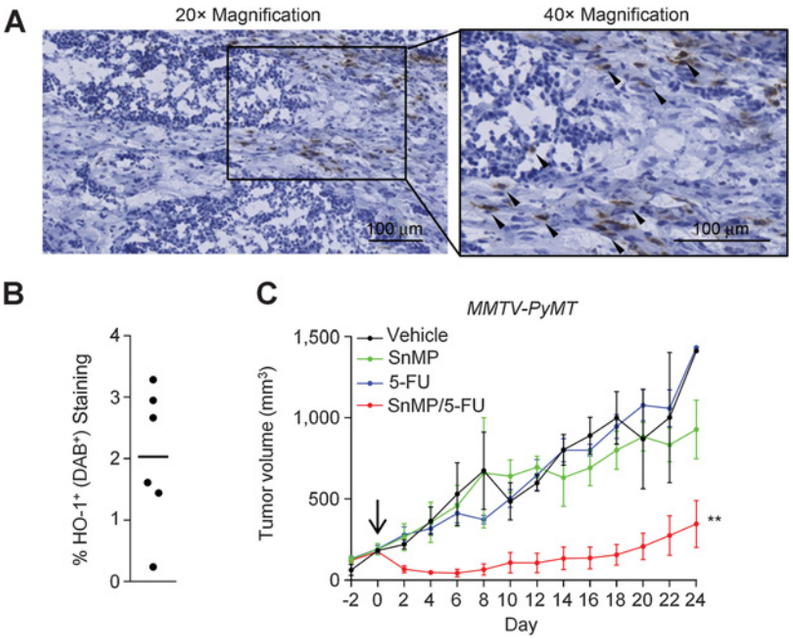

Figure 1.

SnMP synergizes with 5-FU to achieve disease remission and control of tumor growth. **A,** Representative untreated *MMTV-PyMT* tumor section stained using hematoxylin and antibodies against HO-1 (brown). Arrowheads denote examples of HO-1$^+$ cells. **B,** Quantification of HO-1$^+$ staining in untreated *MMTV-PyMT* tumors (average across multiple sections), each dot represents an individual tumor. **C,** Growth curves of established spontaneous tumors in *MMTV-PyMT* mice that had received SnMP (25 μmol/kg/day; $n = 6$) or vehicle ($n = 5$), with or without 5-FU (40 mg/kg/5 days; $n = 6$ alone, $n = 4$ with SnMP). Growth curves are presented as mean ± s.e.m. Tumor growth curves were compared for differences using the "compareGrowthCurves" permutation test (35). **, $P < 0.01$.

absence of tumoral CD8$^+$ T-cells, demonstrating that the mechanism of tumor control was CD8$^+$ T-cell dependent (Fig. 2A). Because tumor remission was observed within 48 hours of the initiation of treatment, a role of chemotherapy in priming an antitumor immune response was unlikely (22). This suggested that the effects were more likely mediated by modulation of an ongoing spontaneous response. *MMTV-PyMT* tumors which had been acutely treated for 36 hours were analyzed to characterize the earliest biological changes at the point at which tumors had started to regress (Fig. 2B). Tumors were excised and enzyme-digested to assess the prevalence of lymphocytes in the tumor microenvironment (Fig. 2C and D). In the treatment groups containing 5-FU, there was a significant influx of CD4$^+$ and CD8$^+$ T-cells (Fig. 2D), whereas SnMP as a single agent had no effect on the tumoral accumulation of lymphocytes (Fig. 2D). This was a specific influx of lymphocytes and not an artifact of a changing microenvironment, as there was no difference in the tumoral abundance of TAMs, monocytes, neutrophils or CAFs (Fig. 2E). CD3$^+$ CD8$^{+/-}$ T cells could also be observed infiltrating the tumor tissue by immunofluorescence staining of frozen tumor sections (Fig. 2F and G and Supplementary Fig. S2C). This T-cell influx coincided with a tumoral increase in expression of the T-cell chemokines *Cxcl9*, *10*, and *11*, suggesting that this was a chemotactic response (Fig. 2H). There was no increase in expression of other genes which have been associated with resistance to chemotherapy such as VEGF, cathepsin proteases or IL-12 (ref. 41; Supplementary Fig. S2D). We therefore assessed the activation status of the tumor-infiltrating CD8$^+$ T-cells. We found that there was an increased prevalence of CD8$^+$ T-cells capable of expressing the effector molecule granzyme B (Fig. 2I). Moreover, *ex vivo* inhibition of HO increased the proportion of tumoral CD8$^+$ T-cells capable of producing the effector cytokines IFNγ and TNFα in response to phorbol myristate acetate (PMA)/ionomycin stimulation (Fig. 2J), indicating that HO was suppressing the effector functions of the infiltrating CD8$^+$ T-cells. The therapeutic synergy of combining chemotherapy and SnMP was not tumor model or chemotherapy class specific, as SnMP also improved the immune-mediated effects of paclitaxel in the orthotopic 4T1 model of murine mammary adenocarcinoma (Supplementary Fig. S2E and S2F). These data suggest that SnMP could be regarded as an innate immune checkpoint therapy in murine models of breast cancer.

SnMP targets myeloid HO-1 in the tumor microenvironment

In *MMTV-PyMT* tumors, 87.3 ± 8.0% of HO-1$^+$ events could be found colocalizing with the TAM marker F4/80 by immunofluorescence staining of frozen tumor sections (Fig. 3A and B; Supplementary Fig. S3A). TAMs were also the most abundant stromal cell type in *MMTV-PyMT* tumors (Fig. 3C), permitting the conclusion that TAMs were the predominant tumoral source of the enzyme. In agreement, F4/80$^+$ TAMs were the primary source of HO-1 in orthotopic 4T1 tumors (Supplementary Fig. S3B and S3C). TAMs play a pivotal role in resistance to chemotherapy (42–44) and facilitate relapse after the cessation of treatment (45). We considered whether TAM-derived HO-1 might have accounted for these observations, and whether TAM-derived HO-1 mediated the therapeutic efficacy of SnMP. To investigate this, the *Hmox1* gene was specifically inactivated in the myeloid lineage by crossing the *MMTV-PyMT* transgene to a mouse carrying a *loxP* flanked *Hmox1* gene (25) and cre recombinase driven by the myeloid-specific integrin CD11b (*Itgam*) promoter (26). This resulted in a 64% ± 4.6% reduction in macrophage expression of HO-1 (Supplementary Fig. S4). Myeloid-specific inactivation of HO-1 did not affect the latency of tumor establishment (Fig. 3D) nor tumor growth thereafter (Fig. 3E). However, administration of 5-FU to *cre*$^+$ mice in which myeloid-derived HO-1 had been inactivated resulted in tumor regression and long-term control of tumor growth, mirroring the effects of SnMP treatment (Fig. 1C). Inactivation of myeloid HO-1 did not affect the abundance of TAMs in terminal size tumors (Fig. 3F), nor the abundance of CD8$^+$ T-cells (Fig. 3G). However, in line with the *ex vivo* effects of HO inhibition (Fig. 2J), HO-1 inactivation resulted in an increased proportion of tumoral CD8$^+$ T-cells capable of producing the effector molecules IFNγ and TNFα

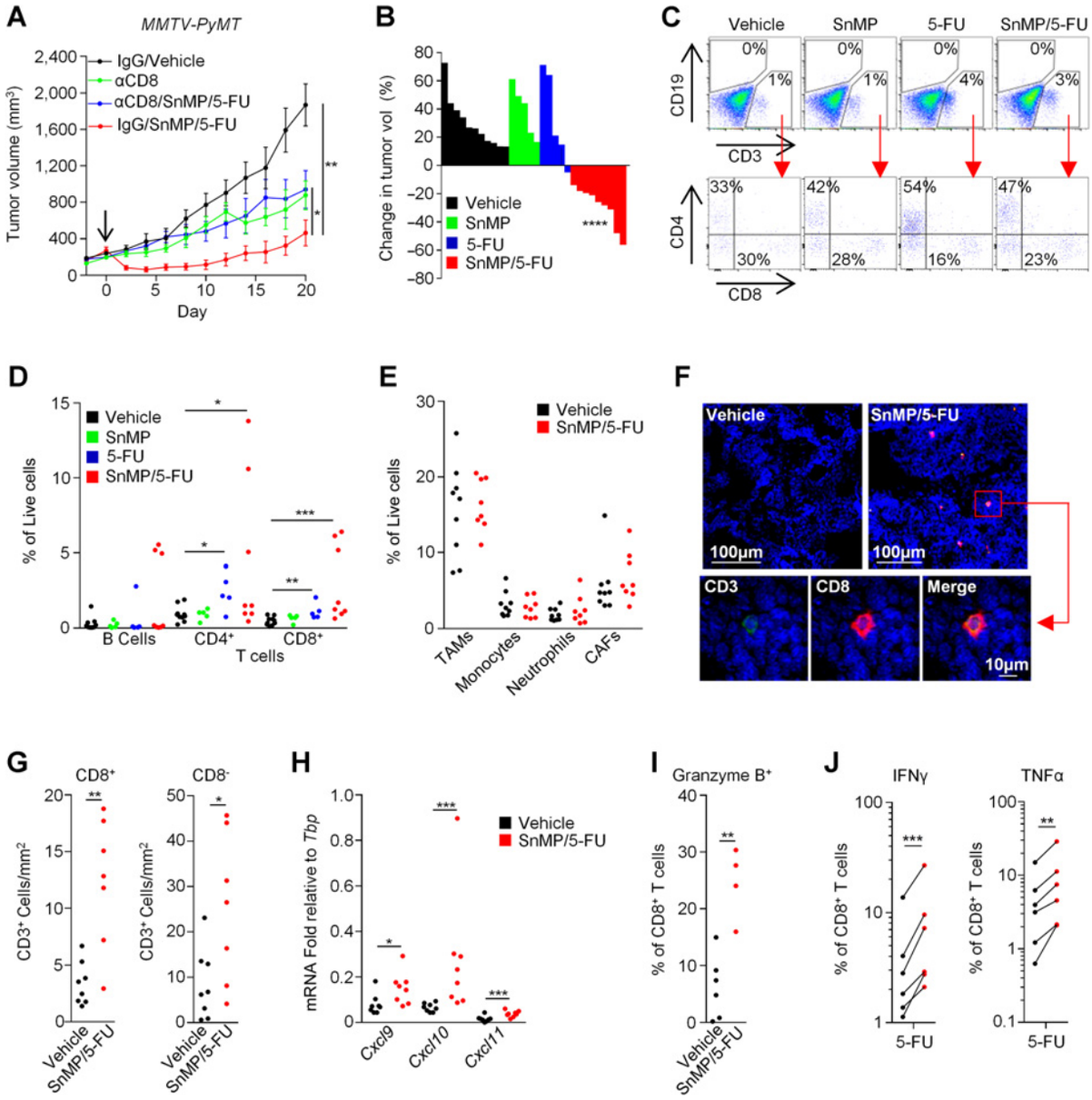

Figure 2.

HO-1 represents an innate immune checkpoint for chemotherapy-elicited CD8$^+$ T cells. **A,** Growth curves of established spontaneous tumors in *MMTV-PyMT* mice that had received immune-depleting anti-CD8α IgG or isotype control IgG. At day zero (marked by arrow) mice were given SnMP (25 µmol/kg/day) and 5-FU (40 mg/kg/5 days) or their respective vehicles (IgG/SnMP/5-FU $n = 5$, all other groups $n = 4$). **B–J,** Effect of 36 hours SnMP (25 µmol/kg/24 hours) and/or 5-FU (40 mg/kg/day 0) or respective vehicle treatment on 500 mm^3 autochthonous *MMTV-PyMT* tumors. **B,** Waterfall plot showing the percentage change in tumor growth over the 36 hour period, each bar represents a tumor from an individual mouse. **C,** Flow cytometry gating strategy for live B cells (CD19$^+$) and CD4$^+$ and CD8$^+$ T-cells (CD3$^+$) in the indicated groups. **D,** Quantitation of lymphocytes from vehicle ($n = 8$–9), where compared with that of SnMP ($n = 5$), 5-FU ($n = 5$), and SnMP/5-FU ($n = 8$)–treated mice. **E,** Quantitation of stromal cell populations in tumors of vehicle ($n = 9$) and SnMP/5-FU ($n = 8$) treated mice. **F,** Representative *MMTV-PyMT* tumor sections from vehicle and SnMP/5-FU–treated mice stained with DAPI (nuclei, blue) and antibodies against CD3 (green) and CD8 (red), larger area images shown Supplementary Fig. S2C. **G,** Quantitation of CD3$^+$ CD8$^{+/-}$ events in (**F**) across multiple sections and tumors of vehicle ($n = 8$) or SnMP/5-FU ($n = 7$)–treated mice. **H,** Relative tumoral mRNA expression for the indicated T- cell chemokines of mice treated with vehicle or SnMP/5-FU ($n = 8$) as described in **B**. **I,** Percentage of live CD8$^+$ T-cells expressing granzyme B as assessed by flow cytometry of enzyme-dispersed tumors from mice treated with vehicle ($n = 6$) or SnMP/5-FU ($n = 4$) as described in (**B**). **J,** Percentage of live CD8$^+$ T-cells producing IFNγ and TNFα as assessed by flow cytometry of enzyme-dispersed *MMTV-PyMT* tumors from mice treated with 5-FU stimulated *ex vivo* with PMA/ionomycin ($n = 6$) in the absence (black) or presence (red) of SnMP (25 µmol/L). Each dot pair represents an individual tumor and mouse; line joins the points from the same tumor. Growth curves are presented as mean ± s.e.m. Tumor growth curves were compared for differences using the "compareGrowthCurves" permutation test (35). *, $P < 0.05$; **, $P < 0.01$; ***, $P < 0.001$; ****, $P < 0.0001$.

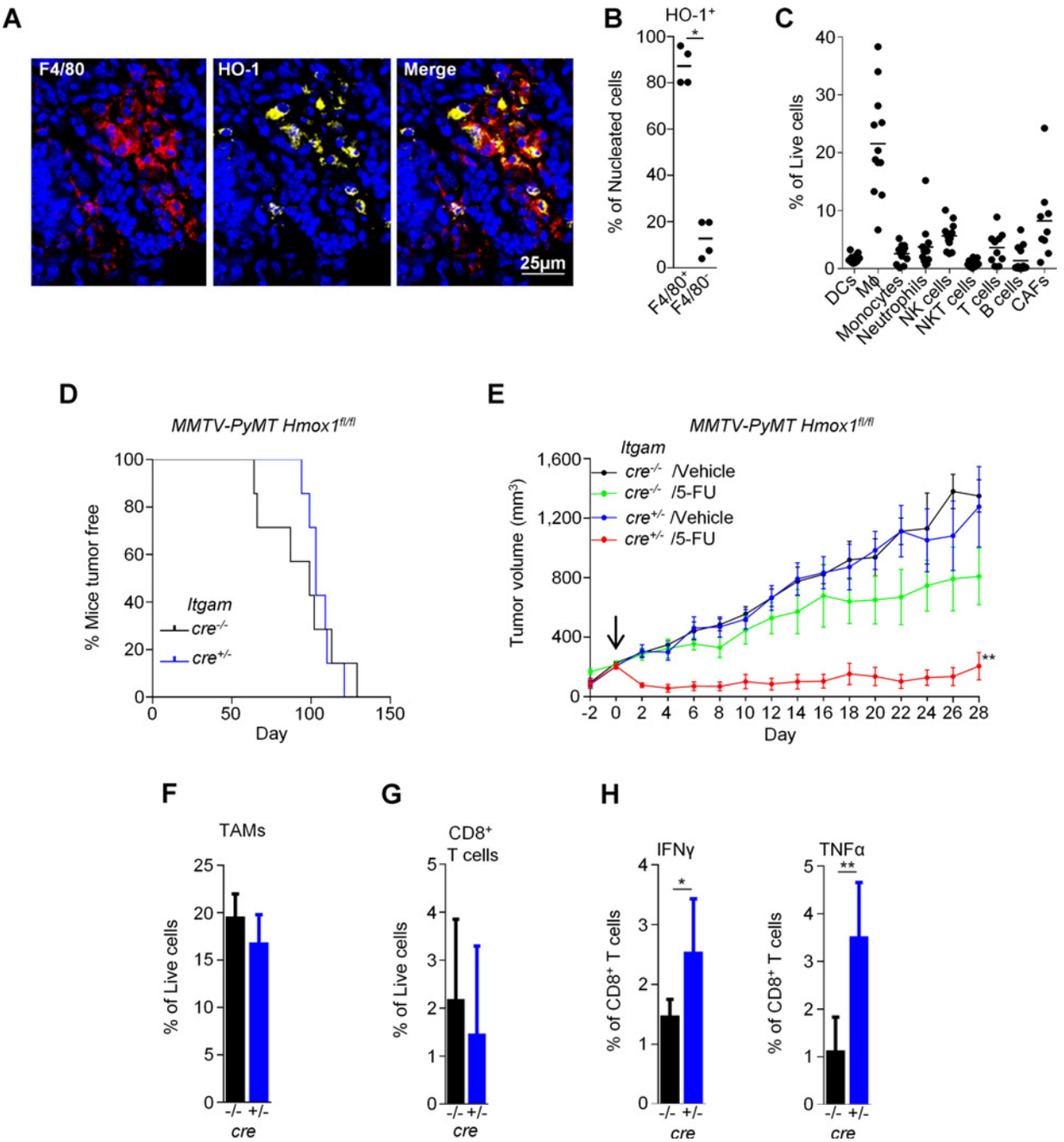

Figure 3.

Genetic inactivation of myeloid-derived HO-1 is sufficient to account for the effects of SnMP. **A,** Representative *MMTV-PyMT* tumor section stained using DAPI (nuclei, blue) and antibodies against F4/80 (red) and HO-1 (yellow). **B,** Quantitation of the HO-1$^+$ events colocalizing with F4/80 in untreated *MMTV-PyMT* tumors (average across multiple sections and fields), each dot represents an individual tumor. **C,** Abundance of specific stromal cell populations in live tumoral cells. Markers used to identify the specific stromal populations are described in Materials and Methods. Each dot represents an individual tumor from an individual mouse. **D** and **E,** Conditional inactivation of HO-1 in the myeloid lineage was achieved in *MMTV-PyMT* mice carrying *Hmox1*$^{fl/fl}$ *Itgam*^{cre} loci. *Cre*$^-$ mice were used as controls. Kaplan–Meier plot marking the day of tumor establishment of *cre*$^-$ (black; $n = 6$) and *cre*$^+$ (blue; $n = 12$) mice (**D**) and tumor growth curves in mice with and without *cre*, treated with 5-FU (40 mg/kg/5 days) or vehicle control (vehicle *cre*$^-$ $n = 7$, vehicle *cre*$^+$ $n = 6$, 5-FU *cre*$^-$ $n = 6$, 5-FU *cre*$^+$ $n = 4$ mice; **E**). **F–H,** Abundance of live F4/80$^+$ TAMs (**F**) CD8$^+$ T-cells (**G**) and percentage of live tumoral CD8$^+$ T-cells expressing IFNγ and TNFα (**H**) as assessed using flow-cytometry analysis of terminal size tumors from vehicle treated *cre*$^+$ ($n = 4$–5) or *cre*$^-$ ($n = 5$) mice stimulated *ex vivo* with PMA/ionomycin. Growth curves are represented as mean ± SEM and bar charts as mean + SD. Tumor growth curves were compared for differences using the "compareGrowthCurves" permutation test (35). *, $P < 0.05$; **, $P < 0.01$.

(Fig. 3H), demonstrating that SnMP was most likely targeting myeloid HO-1 activity to alleviate the suppression of the chemotherapy-elicited $CD8^+$ T-cell response.

HO-1 is associated with poor prognosis in patients receiving chemotherapy

In light of these observations, we investigated whether *HMOX1* expression had any prognostic value in patients. In the BreastMark dataset (28), *HMOX1* expression was associated with poor prognosis, especially in patients receiving chemotherapy (Fig. 4A and B) with a hazard ratio of 2.15 ($P = 0.003$). *HMOX1* was one of the genes most highly associated with poor prognosis in this patient group (Supplementary Fig. S5A). In contrast, *HMOX1* had no association with survival in patients that had not received chemotherapy (Fig. 4C). The same association was found using the Kaplan–Meier Plotter dataset (ref. 29; Fig. 4D–F). This association was specific to *HMOX1*, and not a general result of enhanced infiltration of myeloid cells or macrophages in these tumors, since the myeloid associated genes *CD14* and *ITGAM* had no prognostic value (Supplementary Fig. S5B and S5C). The absence of an effect of *HMOX1* expression in patients that had not received chemotherapy was also not due to lower grade of disease in this subset (Fig. 4G–I). This association between high *HMOX1* expression and poor prognosis also applied to gastric (Fig. 4J–L) and lung cancer (Supplementary Fig. S5D) patients receiving chemotherapy, but did not apply to melanoma patients (Supplementary Fig. S5E), suggesting that the prognostic value of HO-1 may depend on the specific tumor type. In accordance with our preclinical data, these observations suggest a detrimental role of HO-1 expression in patients receiving chemotherapy.

Myeloid cells are a major tumoral source of *HMOX1* expression in human breast cancer

As HO-1 was prognostic for patients receiving chemotherapy, and because our preclinical models of breast cancer had suggested that TAMs were the major tumoral source of HO-1, we investigated whether these observations might translate to the clinic. We therefore analyzed a published single-cell RNA-seq dataset of 509 cells taken from 11 patients with invasive ductal carcinoma of the breast who had undergone breast-conserving surgery or total mastectomy (34). Using an RNA-seq analysis pipeline (see Supplementary Materials and Methods) we grouped cells based on their transcriptomic profiles, using non-linear dimensionality reduction [t-stochastic nearest neighbor embedding (tSNE)] followed by density based clustering (Fig. 5A, Supplementary Figs. S6 and S7). Clusters of cells were annotated by their respective cell lineages based upon their distinguishable preferentially expressed marker genes (Supplementary Table S1). Within each cluster group we assessed expression of *HMOX1*. In agreement with our observations in preclinical models of breast cancer, *HMOX1* expression was most prevalently expressed in the myeloid cell population (Fig. 5B). Of the myeloid cells analyzed, 67% had detectable *HMOX1* expression, whereas only 28% of epithelial/tumor cells had detectable *HMOX1* expression. Although this analysis does not account for the overall abundance of the various cells types, it does demonstrate that myeloid cells are a major tumoral source of the enzyme in human breast cancer. Myeloid cells were also a major tumoral source of the other checkpoint molecules *PDL1* and *PDL2* in human cancer (Fig. 5C and D), suggesting that the myeloid population could play a key role in immune-regulation in these tissues. To confirm that HO-1 protein can be detected in myeloid cells within the breast tissue, tumor sections of human mammary adenocarcinoma were stained for CD11b and HO-1 by immunofluorescence. A population of $CD11b^+$ (Fig. 6A and Supplementary Fig. S8A) and $CD14^+$ (Supplementary Fig. S8B) myeloid cells expressed HO-1 in these tumors confirming that *HMOX1* could be found translated to HO-1 protein in these cells. Using the METABRIC dataset of breast cancer transcriptomes (33), we separated the upper and lower quartiles of *HMOX1* expression in the search for genes co-regulated with *HMOX1*. The group patient characteristics are presented in Supplementary Table S2. *HMOX1* expression was found to be closely associated with myeloid markers *CD163*, *LYZ*, *CD14*, *CD68*, and *ITGAM* (Fig. 6B), which was in agreement with the single-cell RNA-seq dataset. This was not representative of a broader stromal association, as the neutrophil marker *SELL* was only weakly associated and *ELANE* was not associated with *HMOX1* expression. Collectively, these data demonstrate that in breast cancer, myeloid cells represent a major tumoral source of *HMOX1* expression as well as of other checkpoint inhibitor genes such as *PDL1* and *PDL2*.

The hierarchical structure of immune checkpoints in the tumor influences the therapeutic response to immune checkpoint blockade therapy

As HO-1 is an inducible protein and is expressed in response to various stimuli (5, 6), we investigated whether expression of *HMOX1* could be associated with any common features in the tumor microenvironment using the METABRIC dataset (33). Interestingly, the tumors with the highest *HMOX1* expression were associated with an immunologically "hot" gene signature (Fig. 6C) and had higher expression of the lymphocyte associated genes *CD19*, *CD4* and *CD8A* (Fig. 6D). This association has previously been described for PD-L1 (46). Indeed, in human breast cancer, the tumors expressing the highest levels of *PDL1* and *PDL2* also had significantly higher *HMOX1* expression (Fig. 6E). This raised the possibility that redundancy may exist between these immune checkpoint molecules, which could compromise the therapeutic efficacy of the respective monotherapies targeting HO-1 and PD-1. *MMTV-PyMT* tumors were therefore assessed for PD-1 and PD-L expression. PD-1 expression could be detected on 17% of tumoral $CD8^+$ T-cells in this model (Fig. 6F), which paralleled the observations in human breast cancer, where on average 19% of tumor-infiltrating $CD8^+$ T-cells express PD-1 (47). Administration of 5-FU did not affect the prevalence of PD-1 on the $CD8^+$ T-cell population in the *MMTV-PyMT* model (Fig. 6F). As was observed in the human breast cancer dataset (Fig. 5C and D), PD-L1/-L2 were predominantly expressed on the TAM population (Fig. 6G). Because the *MMTV-PyMT* model mirrored the human disease, the biological consequence of immune checkpoint co-expression was analyzed in *MMTV-PyMT* mice bearing large (approximately 800 mm^3) tumors, a size that would permit analysis of potential synergistic effects of combination therapy. PD-1 blockade suppressed tumor growth when compared with vehicle treatment, but did not result in remission of the disease, and this was not enhanced by the addition of 5-FU (Fig. 6H). Administration of SnMP alongside 5-FU was more efficacious than PD-1 blockade in *MMTV-PyMT* tumors (Fig. 6H). Combining the three therapies did not improve the response compared to SnMP/5-FU (Fig. 6H), suggesting that, despite the presence of $PD\text{-}1^+$ $CD8^+$ T-cells and PD-L1/2 expression in the tumor microenvironment, HO-1 represented a hierarchically

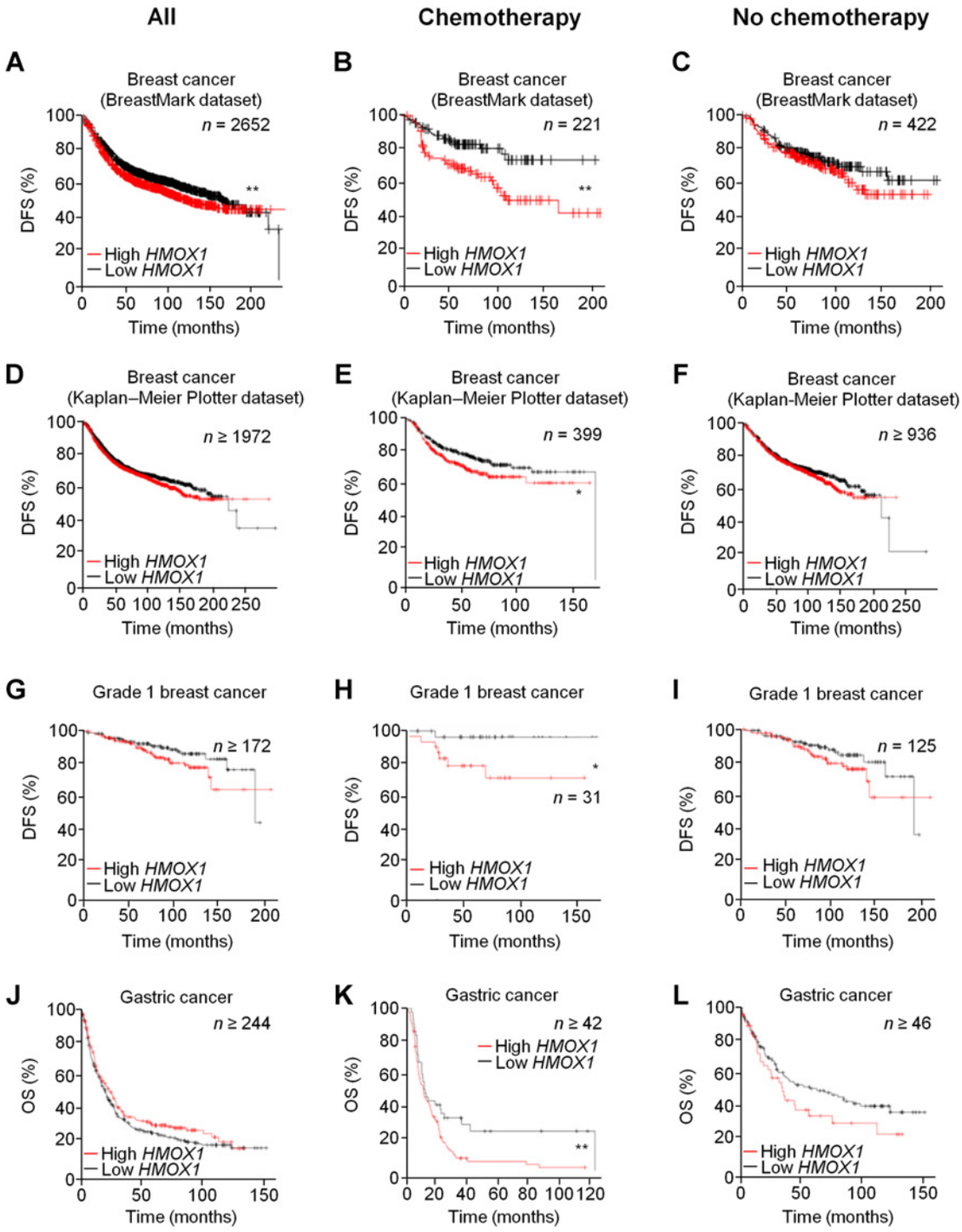

Figure 4.

HMOX1 expression is associated with poor prognosis in chemotherapy-treated patients. Kaplan–Meier survival curves showing disease-free survival (DFS) of breast cancer patients (**A–I**) or overall survival (OS) of gastric cancer patients (**J–L**) with low (black) and high (red) tumoral expression of *HMOX1*, in the entire datasets (left column), in patients receiving chemotherapy (middle column) and in patients not receiving chemotherapy (right column). Data were generated using Breastmark (ref. 28; **A–C**) or Kaplan–Meier plotter (refs. 29, 31; **D–L**) datasets.*, $P < 0.05$; **, $P < 0.01$.

more important immune checkpoint. The same experiment was conducted in orthotopic 4T1 tumors using paclitaxel (Supplementary Fig. S9). In 4T1 tumors 25.8 ± 6.4% of $CD8^+$ T-cells expressed PD-1 (Supplementary Fig. S9A and S9B), and in agreement with the *MMTV-PyMT* tumors and the human disease, PD-L1/2 were predominantly expressed by the TAMs

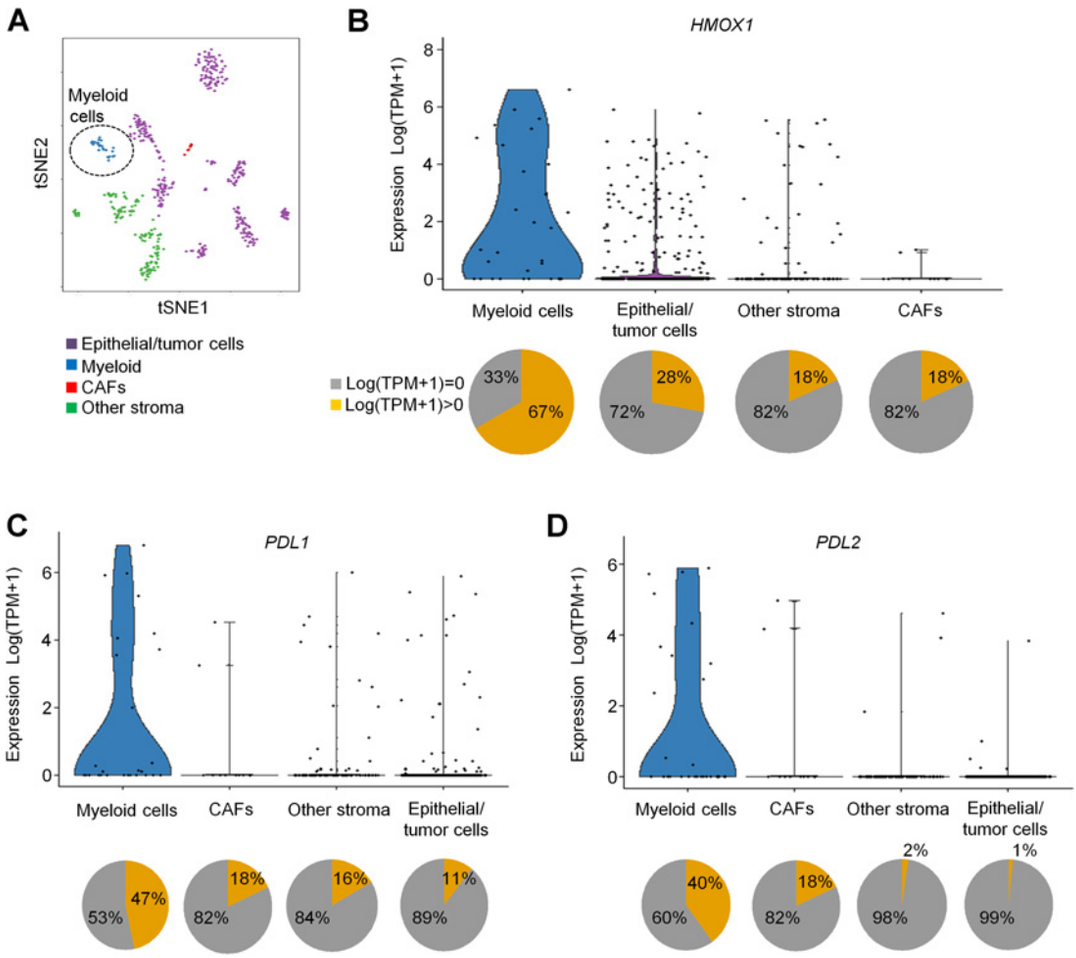

Figure 5.

Single-cell RNA-seq reveals myeloid cells to be the major tumoral source of HO-1 and PD-Ls in human breast cancer. Single-cell transcriptomic profiles from 11 breast cancer patients in a recently published dataset (34) were analyzed. **A**, tSNE analysis showing the cellular clustering and their assigned lineage category as myeloid cells ($n = 30$, blue), epithelial/tumor cells ($n = 326$, purple), CAFs ($n = 11$, red), and other stroma ($n = 130$, green). The myeloid cell cluster is defined by genes *LYZ, CD14, FCER1G, CD163* (as highlighted in Supplementary Table S1). **B,** Violin plots showing the raw [Log(TPM+1)] expression of *HMOX1* in the different groups (top), and pie charts showing the percentage of events with detectable expression of *HMOX1* (bottom). **C** and **D,** The same analysis as **B** but for the expression of *PDL1* (*CD274*; **C**) and *PDL2* (*PDCD1LG2*; **D**). Groups of cells are presented in order of average gene expression [Log(TPM+1)] from highest (left) to lowest (right) in (**B–D**). The analysis pipeline and testing method for single-cell RNA-Seq is described in full within the Supplementary Materials and Methods section.

(Supplementary Fig. S9C). Treatment of mice bearing established 4T1 tumors with SnMP and/or PD-1 blockade alongside paclitaxel resulted in an equivalent control of tumor growth in this model (Supplementary Fig. S9D). Together, these observations suggest that HO-1 represents an important immune checkpoint which can suppress chemotherapy-elicited antitumor immune responses. This highlights the clinical need to evaluate SnMP as an immune checkpoint therapy, especially in patients receiving chemotherapy.

Discussion

In this study, we have demonstrated that SnMP has significant potential to be re-evaluated as a novel immune checkpoint therapy in patients receiving immune-stimulating chemotherapy (illustrated in Supplementary Fig. S10). Chemotherapeutics have been used for the treatment of cancer for nearly 70 years. Although these drugs were first administered to patients for their ability to target the cell cycle, their immune-stimulating properties may underlie a significant proportion of their clinical efficacy (21–24). As we demonstrate here, the efficacy of these therapies can be compromised by tumor immune checkpoints, a concept that is supported by the observation that inhibition of the checkpoint molecules PD-1 and CTLA-4 improves the response to chemotherapy (24). Accordingly, we have shown that chemotherapies used in cancer treatment such as 5-FU and paclitaxel provide valuable tools for eliciting antitumor immune responses. Importantly, this study has demonstrated that chemotherapy-elicited $CD8^+$ T-cell responses are sufficient to achieve long-term immunological control of tumor growth when combined with appropriate immune checkpoint blockade therapy. These data also suggest that HO-1 activity might contribute to unresponsiveness

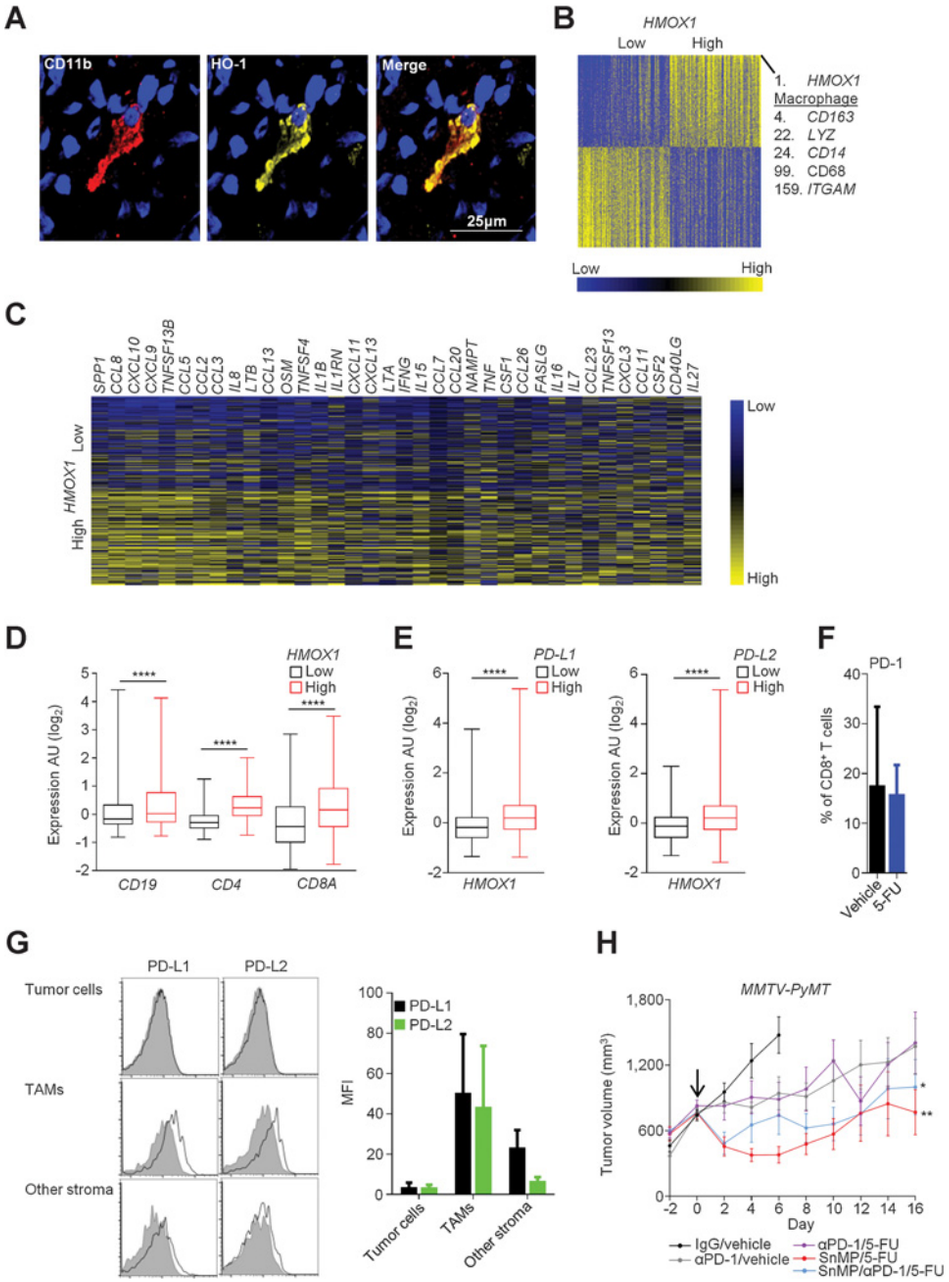

Figure 6.

SnMP can be more efficacious than PD-1 blockade as an immune checkpoint therapy approach alongside chemotherapy. **A,** Representative human adenocarcinoma frozen section stained with DAPI (nuclei, blue) and antibodies against CD11b (red) and HO-1 (yellow). **B,** Heatmap of the top and bottom quartile of *HMOX1* expression in human mammary adenocarcinoma from the METABRIC dataset (33) displaying 6391 genes which were significantly differentially expressed ($n = 388$). Marked are the ranking of genes commonly associated with TAMs. **C,** Heatmap of genes commonly associated with inflammation extracted from **B**. **D,** Box and whisker plots for expression of the indicated lymphocyte markers in *HMOX1* high/low tumors taken from **B**. **E,** Box and whisker plots for the expression of *HMOX1* within the upper (high) and bottom (low) deciles of expression of the indicated checkpoint molecules in human mammary adenocarcinoma ($n = 214$). Both **D** and **E** were normalized against the median expression for the indicated gene. **F,** Quantitation of the proportion of $CD8^+$ T-cells that were $PD\text{-}1^+$ in *MMTV-PyMT* tumors acutely treated with 5-FU (blue; $n = 5$) or vehicle (black; $n = 14$). **G,** Representative histograms (left) and quantification of median fluorescence intensity (MFI) for the positive stain with isotype staining MFI subtracted (right) of surface PD-L1 and PD-L2 expression on gated live tumor cells ($CD45^-$, $Thy1^-$, $CD31^-$), $F4/80^+$ TAMs or remaining stroma in *MMTV-PyMT* tumors ($n = 5$). Open histograms represent specific antibody staining and gray histograms represent isotype antibody staining. **H,** Growth curves of large (800 mm^3) *MMTV-PyMT* tumors treated with anti–PD-1 (12 mg/kg/3 days), isotype control IgG (12 mg/kg/3 days) or SnMP (25 μmol/kg/day) alongside 5-FU (40 mg/kg/5 days; $n = 4$) or vehicle ($n = 5$). Arrow denotes initiation of treatment. Growth curves are represented as mean ± SEM and bar charts as mean + SD. Tumor growth curves were compared for differences using the "compareGrowthCurves" permutation test (35). The group data presented in **D** and **E** were compared using a Mann–Whitney test. *, $P < 0.05$; **, $P < 0.01$; ****, $P < 0.0001$.

of a group of patients to the current immune checkpoint blockade therapies (1, 2). CO, one of the by-products of heme catabolism, has been demonstrated to have potent immune-suppressive properties through directly modulating cell signaling (48). As such, HO-1 could be regarded as an innate checkpoint compared with PD-1 and CTLA-4, as it does not require receptor-ligand interactions. As only 17% of $CD8^+$ T-cells expressed PD-1 in *MMTV-PyMT* tumors, which mirrored the clinical setting, this might in part explain why HO-1 inhibition was more efficacious than PD-1 blockade, despite the expression of both immune checkpoints in the tumor. In breast cancer, we demonstrate that expression of the genes for both HO-1 and PD-L are most prevalent within the myeloid-stromal compartment. In other cancers PD-L1 and PD-L2 have been described to be widely expressed by tumor cells (49), highlighting the inter-tumor heterogeneity of immune checkpoint expression. Inter- and intra-tumor hierarchy and redundancy of these molecules will ultimately dictate responses to immune checkpoint blockade therapies in the clinic. These observations therefore suggest that the "tolerogenic landscape" of each tumor needs to be considered when implementing immune checkpoint blockade therapies, or that broader drug combinations might be required to achieve efficient immune checkpoint blockade therapy in the greatest number of patients.

SnMP has completed a phase II (b) trial for the treatment of neonatal hyperbilirubinemia as a single bolus dose injection (19). Because of its low toxicity, repeat dosing of SnMP has also been successfully tested clinically (3 doses/week) in two patients with Crigler-Najjar syndrome (20). Repeated SnMP dosing is well tolerated in humans with the most frequent toxicities being mild (and reversible) cutaneous photosensitivity of sun-exposed areas and anemia (20). The human equivalent of the dose of SnMP used in our study is within the range previously administered to patients, making these observations directly clinically relevant. As such, these data support the clinical evaluation of SnMP in cancer, as a novel immunotherapeutic approach to improve the immunological response to chemotherapy by targeting HO-1.

Disclosure of Potential Conflicts of Interest

No potential conflicts of interest were disclosed.

Authors' Contributions

Conception and design: T. Muliaditan, J.F. Spicer, J.N. Arnold
Development of methodology: T. Muliaditan, J.W. Opzoomer, J. Caron, P. Kosti, S. Kordasti, J.N. Arnold
Acquisition of data (provided animals, acquired and managed patients, provided facilities, etc.): T. Muliaditan, J.W. Opzoomer, J. Caron, M. Okesola, A. Tutt, C.E. Gillett, J.M. Burchell, J.N. Arnold
Analysis and interpretation of data (e.g., statistical analysis, biostatistics, computational analysis): T. Muliaditan, J.W. Opzoomer, J. Caron, P. Kosti, M. Van Hemelrijck, A. Grigoriadis, S.F. Madden, J.F. Spicer, J.N. Arnold
Writing, review, and/or revision of the manuscript: T. Muliaditan, J.W. Opzoomer, J. Caron, P. Kosti, M. Van Hemelrijck, F. Dazzi, S.F. Madden, S. Kordasti, S.S. Diebold, J.F. Spicer, J.N. Arnold
Administrative, technical, or material support (i.e., reporting or organizing data, constructing databases): M. Okesola, S. Lall, A. Tutt
Study supervision: J.M. Burchell, S.S. Diebold, J.N. Arnold

Acknowledgments

The authors thank Thomas Hayday and Dr. Yasmin Haque (KCL) for cell sorting and flow cytometry assistance, Dr. Hans Garmo (senior medical statistician, KCL) for his advice on the application of statistics used in this study, Charlotte Saxby for running the Western blot shown in Supplementary Fig. S3C, Dr. Patrycja Gazinska (KCL) for scanning the histology slides, Samantha Arnold for preparing Supplementary Fig. S9, Dr. Morris Muliaditan (University College London) for critical review of the article and the Nikon Imaging Centre KCL for use of their facilities and assistance with confocal microscopy. This work was funded by grants from the European Research Council (335326) and Cancer Research UK (22253) and supported by the Experimental Cancer Medicine Centre at King's College London and the National Institute for Health Research (NIHR) Biomedical Research Centre based at Guy's and St Thomas' NHS Foundation Trust and King's College London.

The costs of publication of this article were defrayed in part by the payment of page charges. This article must therefore be hereby marked *advertisement* in accordance with 18 U.S.C. Section 1734 solely to indicate this fact.

Received September 8, 2017; revised December 1, 2017; accepted January 8, 2018; published OnlineFirst January 16, 2018.

References

1. Sharma P, Allison JP. The future of immune checkpoint therapy. Science 2015;348:56–61.
2. Wolchok JD, Kluger H, Callahan MK, Postow MA, Rizvi NA, Lesokhin AM, et al. Nivolumab plus ipilimumab in advanced melanoma. N Engl J Med 2013;369:122–33.
3. Kim JE, Patel MA, Mangraviti A, Kim ES, Theodros D, Velarde E, et al. Combination therapy with anti-PD-1, anti-TIM-3, and focal radiation results in regression of murine gliomas. Clin Cancer Res 2017;23:124–36.
4. Koyama S, Akbay EA, Li YY, Herter-Sprie GS, Buczkowski KA, Richards WG, et al. Adaptive resistance to therapeutic PD-1 blockade is associated with upregulation of alternative immune checkpoints. Nat Commun 2016;7:10501.
5. Gozzelino R, Jeney V, Soares MP. Mechanisms of cell protection by heme oxygenase-1. Annu Rev Pharmacol Toxicol 2010;50:323–54.
6. Ryter SW, Choi AM. Heme oxygenase-1/carbon monoxide: from metabolism to molecular therapy. Am J Respir Cell Mol Biol 2009;41:251–60.
7. Arnold JN, Magiera L, Kraman M, Fearon DT. Tumoral immune suppression by macrophages expressing fibroblast activation protein-alpha and heme oxygenase-1. Cancer Immunol Res 2014;2:121–6.
8. Tan Q, Wang H, Hu Y, Hu M, Li X, Aodengqimuge, et al. Src/STAT3-dependent heme oxygenase-1 induction mediates chemoresistance of breast cancer cells to doxorubicin by promoting autophagy. Cancer Sci 2015;106:1023–32.
9. Nuhn P, Kunzli BM, Hennig R, Mitkus T, Ramanauskas T, Nobiling R, et al. Heme oxygenase-1 and its metabolites affect pancreatic tumor growth in vivo. Mol Cancer 2009;8:37.
10. Nowis D, Bugajski M, Winiarska M, Bil J, Szokalska A, Salwa P, et al. Zinc protoporphyrin IX, a heme oxygenase-1 inhibitor, demonstrates potent antitumor effects but is unable to potentiate antitumor effects of chemotherapeutics in mice. BMC Cancer 2008;8:197.
11. Di Biase S, Lee C, Brandhorst S, Manes B, Buono R, Cheng CW, et al. Fasting-mimicking diet reduces HO-1 to promote T cell-mediated tumor cytotoxicity. Cancer Cell 2016;30:136–46.
12. Berberat PO, Dambrauskas Z, Gulbinas A, Giese T, Giese N, Kunzli B, et al. Inhibition of heme oxygenase-1 increases responsiveness of pancreatic cancer cells to anticancer treatment. Clin Cancer Res 2005;11:3790–8.
13. Otterbein LE, Bach FH, Alam J, Soares M, Tao Lu H, Wysk M, et al. Carbon monoxide has anti-inflammatory effects involving the mitogen-activated protein kinase pathway. Nat Med 2000;6:422–8.
14. Zhang X, Shan P, Alam J, Fu XY, Lee PJ. Carbon monoxide differentially modulates STAT1 and STAT3 and inhibits apoptosis via a phosphatidylinositol 3-kinase/Akt and p38 kinase-dependent STAT3 pathway during anoxia-reoxygenation injury. J Biol Chem 2005;280:8714–21.
15. Cepinskas G, Katada K, Bihari A, Potter RF. Carbon monoxide liberated from carbon monoxide-releasing molecule CORM-2 attenuates inflammation in the liver of septic mice. Am J Physiol Gastrointest Liver Physiol 2008;294:G184–91.

16. Megias J, Busserolles J, Alcaraz MJ. The carbon monoxide-releasing molecule CORM-2 inhibits the inflammatory response induced by cytokines in Caco-2 cells. Br J Pharmacol 2007;150:977–86.
17. Clavijo PE, Frauwirth KA. Anergic CD8+ T lymphocytes have impaired NF-kappaB activation with defects in p65 phosphorylation and acetylation. J Immunol 2012;188:1213–21.
18. Wong RJ, Vreman HJ, Schulz S, Kalish FS, Pierce NW, Stevenson DK. In vitro inhibition of heme oxygenase isoenzymes by metalloporphyrins. J Perinatol 2011;31Suppl 1:S35–41.
19. Valaes T, Petmezaki S, Henschke C, Drummond GS, Kappas A. Control of jaundice in preterm newborns by an inhibitor of bilirubin production: studies with tin-mesoporphyrin. Pediatrics 1994;93:1–11.
20. Galbraith RA, Drummond GS, Kappas A. Suppression of bilirubin production in the Crigler-Najjar type I syndrome: studies with the heme oxygenase inhibitor tin-mesoporphyrin. Pediatrics 1992;89:175–82.
21. Casares N, Pequignot MO, Tesniere A, Ghiringhelli F, Roux S, Chaput N, et al. Caspase-dependent immunogenicity of doxorubicin-induced tumor cell death. J Exp Med 2005;202:1691–701.
22. Geary SM, Lemke CD, Lubaroff DM, Salem AK. The combination of a low-dose chemotherapeutic agent, 5-fluorouracil, and an adenoviral tumor vaccine has a synergistic benefit on survival in a tumor model system. PLoS ONE 2013;8:e67904.
23. Bracci L, Schiavoni G, Sistigu A, Belardelli F. Immune-based mechanisms of cytotoxic chemotherapy: implications for the design of novel and rationale-based combined treatments against cancer. Cell Death Differ 2014; 21:15–25.
24. Pfirschke C, Engblom C, Rickelt S, Cortez-Retamozo V, Garris C, Pucci F, et al. Immunogenic chemotherapy sensitizes tumors to checkpoint blockade therapy. Immunity 2016;44:343–54.
25. Tzima S, Victoratos P, Kranidioti K, Alexiou M, Kollias G. Myeloid heme oxygenase-1 regulates innate immunity and autoimmunity by modulating IFN-beta production. J Exp Med 2009;206:1167–79.
26. Boillee S, Yamanaka K, Lobsiger CS, Copeland NG, Jenkins NA, Kassiotis G, et al. Onset and progression in inherited ALS determined by motor neurons and microglia. Science 2006;312:1389–92.
27. Kraman M, Bambrough PJ, Arnold JN, Roberts EW, Magiera L, Jones JO, et al. Suppression of antitumor immunity by stromal cells expressing fibroblast activation protein-alpha. Science 2010;330:827–30.
28. Madden SF, Clarke C, Gaule P, Aherne ST, O'Donovan N, Clynes M, et al. BreastMark: an integrated approach to mining publicly available transcriptomic datasets relating to breast cancer outcome. Breast Cancer Res 2013;15:R52.
29. Gyorffy B, Lanczky A, Eklund AC, Denkert C, Budczies J, Li Q, et al. An online survival analysis tool to rapidly assess the effect of 22,277 genes on breast cancer prognosis using microarray data of 1,809 patients. Breast Cancer Res Treat 2010;123:725–31.
30. Gyorffy B, Surowiak P, Budczies J, Lanczky A. Online survival analysis software to assess the prognostic value of biomarkers using transcriptomic data in non-small-cell lung cancer. PLoS ONE 2013;8:e82241.
31. Szasz AM, Lanczky A, Nagy A, Forster S, Hark K, Green JE, et al. Cross-validation of survival associated biomarkers in gastric cancer using transcriptomic data of 1,065 patients. Oncotarget 2016;7:49322–33.
32. Cirenajwis H, Ekedahl H, Lauss M, Harbst K, Carneiro A, Enoksson J, et al. Molecular stratification of metastatic melanoma using gene expression profiling: Prediction of survival outcome and benefit from molecular targeted therapy. Oncotarget 2015;6:12297–309.
33. Curtis C, Shah SP, Chin SF, Turashvili G, Rueda OM, Dunning MJ, et al. The genomic and transcriptomic architecture of 2,000 breast tumours reveals novel subgroups. Nature 2012;486:346–52.
34. Chung W, Eum HH, Lee HO, Lee KM, Lee HB, Kim KT, et al. Single-cell RNA-seq enables comprehensive tumour and immune cell profiling in primary breast cancer. Nat Commun 2017;8:15081.
35. Elso CM, Roberts LJ, Smyth GK, Thomson RJ, Baldwin TM, Foote SJ, et al. Leishmaniasis host response loci (lmr1–3) modify disease severity through a Th1/Th2-independent pathway. Genes Immun 2004;5:93–100.
36. Guy CT, Cardiff RD, Muller WJ. Induction of mammary tumors by expression of polyomavirus middle T oncogene: a transgenic mouse model for metastatic disease. Mol Cell Biol 1992;12:954–61.
37. Lin EY, Jones JG, Li P, Zhu L, Whitney KD, Muller WJ, et al. Progression to malignancy in the polyoma middle T oncoprotein mouse breast cancer model provides a reliable model for human diseases. Am J Pathol 2003;163:2113–26.
38. Longley DB, Harkin DP, Johnston PG. 5-fluorouracil: mechanisms of action and clinical strategies. Nat Rev Cancer 2003;3:330–8.
39. Ugel S, Peranzoni E, Desantis G, Chioda M, Walter S, Weinschenk T, et al. Immune tolerance to tumor antigens occurs in a specialized environment of the spleen. Cell Rep 2012;2:628–39.
40. Cao Z, Zhang Z, Huang Z, Wang R, Yang A, Liao L, et al. Antitumor and immunomodulatory effects of low-dose 5-FU on hepatoma 22 tumor-bearing mice. Oncol Lett 2014;7:1260–4.
41. Ruffell B, Coussens LM. Macrophages and therapeutic resistance in cancer. Cancer Cell 2015;27:462–72.
42. Paulus P, Stanley ER, Schafer R, Abraham D, Aharinejad S. Colony-stimulating factor-1 antibody reverses chemoresistance in human MCF-7 breast cancer xenografts. Cancer Res 2006;66:4349–56.
43. DeNardo DG, Brennan DJ, Rexhepaj E, Ruffell B, Shiao SL, Madden SF, et al. Leukocyte complexity predicts breast cancer survival and functionally regulates response to chemotherapy. Cancer Discov 2011;1:54–67.
44. Ruffell B, Chang-Strachan D, Chan V, Rosenbusch A, Ho CM, Pryer N, et al. Macrophage IL-10 blocks CD8+ T cell-dependent responses to chemotherapy by suppressing IL-12 expression in intratumoral dendritic cells. Cancer Cell 2014;26:623–37.
45. Hughes R, Qian BZ, Rowan C, Muthana M, Keklikoglou I, Olson OC, et al. Perivascular M2 macrophages stimulate tumor relapse after chemotherapy. Cancer Res 2015;75:3479–91.
46. Spranger S, Spaapen RM, Zha Y, Williams J, Meng Y, Ha TT, et al. Up-regulation of PD-L1, IDO, and T(regs) in the melanoma tumor microenvironment is driven by CD8(+) T cells. Sci Transl Med 2013;5:200ra116.
47. Buisseret L, Garaud S, de Wind A, Van den Eynden G, Boisson A, Solinas C, et al. Tumor-infiltrating lymphocyte composition, organization and PD-1/PD-L1 expression are linked in breast cancer. Oncoimmunology 2017;6:e1257452.
48. Minamoto K, Harada H, Lama VN, Fedarau MA, Pinsky DJ. Reciprocal regulation of airway rejection by the inducible gas-forming enzymes heme oxygenase and nitric oxide synthase. J Exp Med 2005;202:283–94.
49. Latchman Y, Wood CR, Chernova T, Chaudhary D, Borde M, Chernova I, et al. PD-L2 is a second ligand for PD-1 and inhibits T cell activation. Nat Immunol 2001;2:261–8.